



Pathogenesis Study of Enterovirus 71 Using a Novel Human SCARB2 Knock-In Mouse Model

 Yuefei Jin,^a Tiantian Sun,^a Guangyuan Zhou,^a Dong Li,^a Shuaiyin Chen,^a Weiguo Zhang,^{a,b} Xueyuan Li,^c Rongguang Zhang,^a Haiyan Yang,^a Guangcai Duan^a

^aDepartment of Epidemiology, College of Public Health, Zhengzhou University, Zhengzhou, China

^bDepartment of Immunology, Duke University Medical Center, Durham, North Carolina, USA

^cDepartment of Neurosurgery, The First Affiliated Hospital of Zhengzhou University, Zhengzhou, China

ABSTRACT Enterovirus 71 (EV71) can cause a severe hand-foot-mouth disease in children. However, the precise mechanism of EV71-associated disease, particularly the neuropathogenesis and pulmonary disorder, is still not fully understood because no suitable animal models are available. The human scavenger receptor class B, member 2 (hSCARB2), is a cellular receptor for EV71. Here, we generated a novel knock-in (KI) mouse model using the CRISPR/Cas9 system to insert the hSCARB2 gene into the mouse *Rosa26* locus to study the pathogenesis of EV71. The hSCARB2 KI mice infected with clinical isolates of EV71 showed neurological symptoms, such as ataxia, paralysis, and death. Viral replication was detected in mainly astrocytes and a limited number of neurons and microglia, accompanied by gliosis. Vascular leakage and alveoli filled with erythrocytes were detected, suggesting that edema and hemorrhage, which are observed in human patients, also occurred in EV71-infected KI mice. In addition, proinflammatory cytokines and chemokines were significantly increased in the serum of infected KI mice. These pathological features of the KI mice after infection resembled those of EV71 encephalomyelitis in humans. Therefore, our KI mouse model is suitable to study the pathogenesis of EV71 and is of great significance for development of antiviral drugs and vaccines to treat or prevent EV71 infection.

IMPORTANCE Enterovirus 71 (EV71) is associated with severe hand-foot-mouth disease. Recently, outbreaks of EV71 infection with high mortality have been reported in the Asia-Pacific region, posing a great challenge for global public health. To date, the precise mechanism of EV71-induced disease, particularly the neuropathogenesis and respiratory disorders, is still not fully understood because no suitable animal models are available. Human scavenger receptor class B, member 2 (hSCARB2), has been identified as a cellular receptor for EV71. Here, we introduce a novel CRISPR/Cas9-mediated hSCARB2 knock-in (KI) mouse model for the study of EV71 pathogenesis, which is of great significance for the development of antiviral drugs and vaccines.

KEYWORDS enterovirus 71, SCARB2, knock-in, pathogenesis

Hand-foot-mouth disease (HFMD) is extremely contagious and prevalent among infants and children less than 5 years old. Enterovirus 71 (EV71) is a human enterovirus species A of the genus *Enterovirus*, belonging to the family *Picornaviridae* (1). EV71 is considered the main pathogen responsible for HFMD and has triggered several disease outbreaks worldwide with high morbidity and mortality rates since its initial isolation in 1969 (2). Two serious epidemics occurred in Malaysia and Taiwan in the late 1990s, causing numerous infections in children, which were characteristically associated with severe neurological complications and a high rate of fatality (3, 4). Most of

Citation Jin Y, Sun T, Zhou G, Li D, Chen S, Zhang W, Li X, Zhang R, Yang H, Duan G. 2021. Pathogenesis study of enterovirus 71 using a novel human SCARB2 knock-in mouse model. *mSphere* 6:e01048-20. <https://doi.org/10.1128/mSphere.01048-20>.

Editor Angela L. Rasmussen, Georgetown University

Copyright © 2021 Jin et al. This is an open-access article distributed under the terms of the [Creative Commons Attribution 4.0 International license](https://creativecommons.org/licenses/by/4.0/).

Address correspondence to Guangcai Duan, gcduan@zzu.edu.cn.

 Human scavenger receptor class B, member 2 (hSCARB2) has been identified as a cellular receptor for EV71. We introduce a novel CRISPR/Cas9-mediated hSCARB2 knock-in (KI) mouse model for pathogenesis study of EV71.

Received 14 October 2020

Accepted 10 February 2021

Published 10 March 2021

those who died were young, and the majority of them died of cardiopulmonary failure (3–5). Since then, the Asia-Pacific region, including Malaysia, Singapore, South Korea, Japan, and China, has experienced more frequent large-scale EV71-related HFMD epidemics (2). EV71 infection is generally mild and self-limited, but occasionally such infection leads to infection of the central nervous system (CNS) and development of aseptic meningitis, brain stem encephalitis, and acute flaccid paralysis (2–4). Fatal infections develop and progress rapidly and are frequently associated with severe neural complications, pulmonary edema, and hemorrhage, which make clinical management challenging (2–4). To date, the precise mechanisms of EV71-induced disease, particularly neuropathogenesis and lung damage, are still not fully understood.

Nonhuman primate models develop neurological complications similar to those observed in clinical cases, including ataxia, tremor, and flaccid paralysis (6, 7), and pathological lesions are present in the spinal cord, brain stem, cerebellar dentate nucleus, and lung sections (6, 7). However, due to ethical and economic considerations, the use of monkeys to model EV71 infection is not ideal. Neonatal mouse models using non-mouse-adapted virus strains or immunodeficient or immunocompetent mice have been used for EV71 vaccine development and pathogenesis study (8–10). Mouse-adapted virus strains with increased virulence in mice were also developed (11, 12). Unfortunately, the virus mutations, route of viral entry, and immunodeficiency in mice cannot accurately reflect the pathogenesis of human diseases. Thus, a new experimental animal model must be established to overcome these limitations.

As a cellular receptor for EV71, human scavenger receptor class B, member 2 (hSCARB2) plays an essential role in the early steps of viral infection (13). SCARB2, also known as lysosomal integral membrane protein 2, localizes mainly to lysosomes (14) and acts as a receptor for lysosomal targeting of β -glucocerebrosidase (15). Mouse L929 cells transformed with hSCARB2 are susceptible to all human enterovirus species A strains (16, 17), facilitating virion binding, internalization, and uncoating (18), whereas mouse SCARB2 does not function as a receptor for EV71. Importantly, SCARB2 is widely expressed in human tissues, including mouth, esophagus, stomach, duodenum, jejunum, ileum, colon, lung, and brain, and is highly expressed in mucosal epithelia, neurons, glial cells, blood vessels, and the perivascular tissues of the brain (19). Relative to other candidate receptors, SCARB2 seems to be more effective in supporting viral infection (20). Transgenic mice expressing hSCARB2 based on a bacterial artificial chromosome (BAC) are susceptible to EV71 infection (21, 22). Here, we report the generation of a new hSCARB2 knock-in (KI) mouse model using CRISPR/Cas9 for the study of EV71 pathogenesis.

RESULTS

Generation of hSCARB2 KI F0 mice. To generate KI mice expressing hSCARB2, a construct containing the hSCARB2 cDNA was inserted into the mouse *Rosa26* locus (23) through homologous recombination using the CRISPR/Cas9 system (Fig. 1A). As described previously (24, 25), the guide RNA was prepared by *in vitro* transcription (IVT), and potential off-target mutations were analyzed using the CRISPOR software. Before microinjection of the CRISPR/Cas9 machinery designed specifically to target the *Rosa26* locus of B6 mice, fertilized eggs were prepared by superovulation of B6 female mice aged 4 to 6 weeks and fertilization with sperm cells from B6 male mice aged 10 to 12 weeks. Two sets of specific guide RNAs and Cas9 mRNA were coinjected with the targeting construct (Fig. 1B). The engineered eggs were developed in ICR outbred fostered mice and genotyped using mouse tail tip DNA from newborns by PCR and gel electrophoresis (Fig. 1B). As shown in Fig. 1C, 200 fertilized eggs were subjected to microinjection, and 190 live eggs were transplanted, resulting in 10 mice with mutations. To validate genome editing by gene-specific targeting, genomic DNA extracted from tail biopsy specimens was analyzed by PCR. Of these 77 pups, 10 had the hSCARB2 gene (Fig. 1D). These results indicated that hSCARB2 gene was successfully targeted at the *Rosa 26* locus using the CRISPR/Cas9 system.

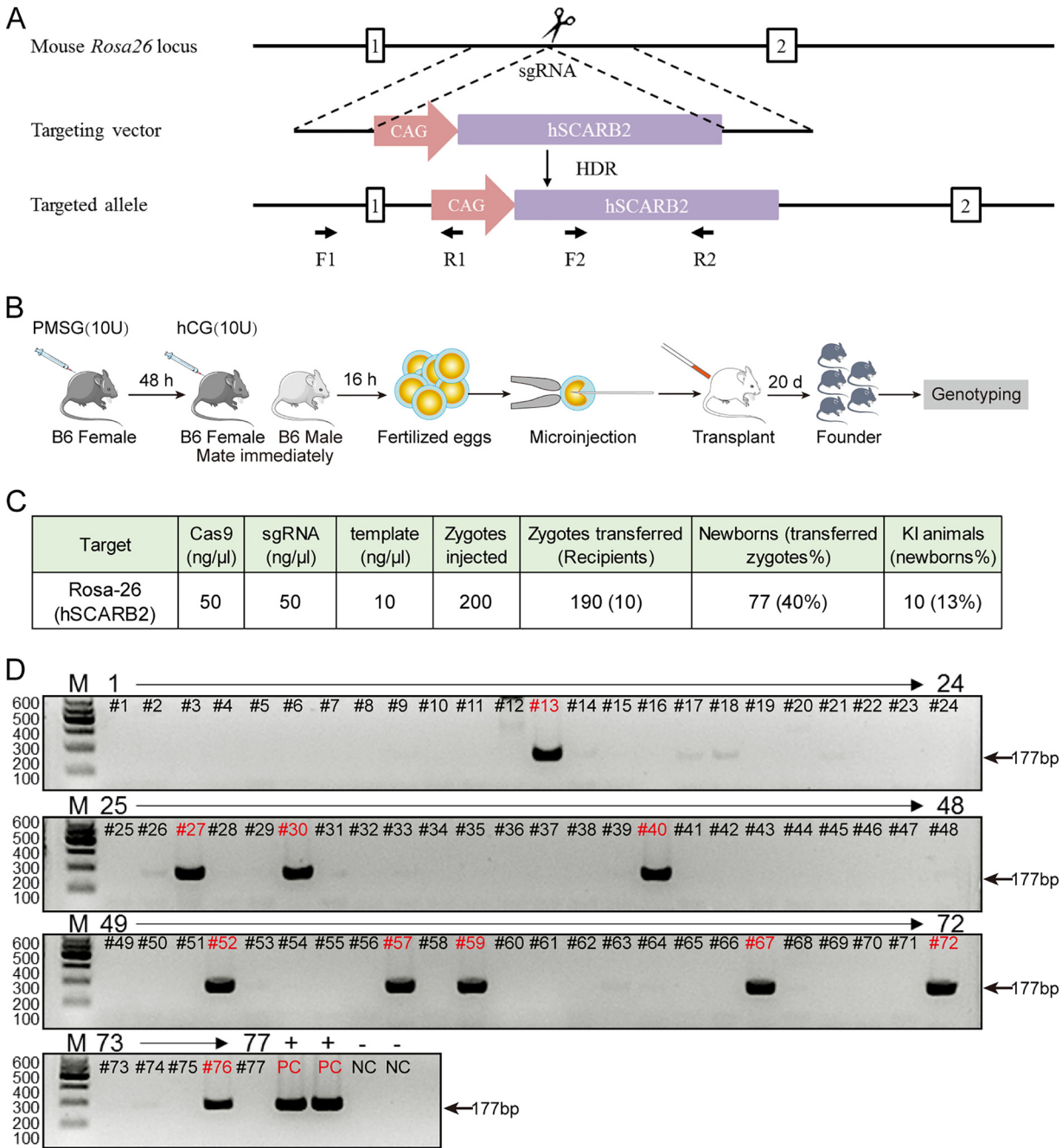


FIG 1 CRISPR/Cas9-mediated KI of *hSCARB2* into the *Rosa26* locus of C57BL/6 zygotes. (A) Diagram of CRISPR/Cas9-mediated KI of the *hSCARB2* gene into the *Rosa26* locus. An expression cassette with the CAG promoter and *hSCARB2* gene was inserted between the homologous arms at the *Rosa26* locus via the CRISPR/Cas9 system. Gene editing was achieved by homology-directed repair (HDR) using the repair template vector for precise insertion of the new sequence. (B) Workflow of the production of *hSCARB2* allele specific KI in F0 mice. (C) Numbers of injected and transferred embryos and newborns generated during establishment of KI mice using the CRISPR/Cas9 system. (D) Genotyping of F0-*hSCARB2* KI mice by using PCR analysis.

Expression profile of *hSCARB2* in human and KI mouse tissues and BMM ϕ . We performed PCR, immunohistochemistry (IHC), and Western blot analysis of human and mouse samples. As shown in Fig. 2A and B, all organs and tissues from *hSCARB2* KI mice at the indicated ages expressed *hSCARB2* mRNA. In contrast, the expression of *hSCARB2* mRNA in the organs and tissues from wild-type (WT) mice was not detectable (Table S2). The expression of *hSCARB2* was detected in all tissues from KI mice using IHC staining with a goat anti-*hSCARB2* polyclonal antibody. Human tissues and

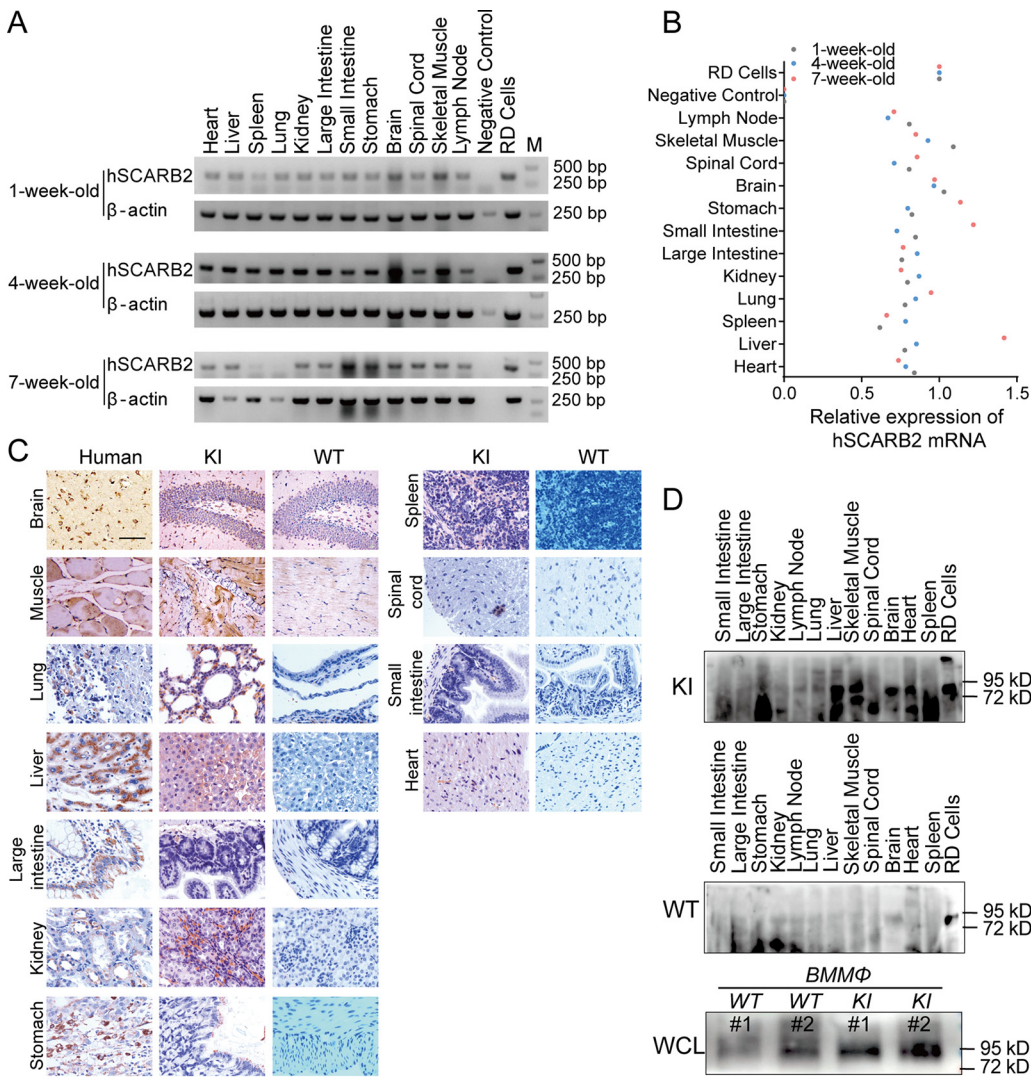


FIG 2 Expression profile of hSCARB2 in human and mouse samples. (A) Expression of hSCARB2 RNA in various tissues from KI mice at indicated ages detected by PCR. (B) Relative expression of hSCARB2 RNA in various tissues from KI mice at the indicated ages. (C) IHC analysis of hSCARB2 expression in human, WT mouse, and KI mouse tissues stained with an anti-human SCARB2 antibody (brown) and counterstained with hematoxylin. (D) Western blot analysis of hSCARB2 expression in various tissues and BMMφ from WT and KI mice.

rhabdomyoma (RD) cells were used as a positive control (Fig. 2C). The hSCARB2 bands with molecular weights ranging from 72 kDa to 95 kDa were detected in the tissues and bone marrow-derived macrophages (BMMφ) from KI mice by Western blotting (Fig. 2D), indicating that hSCARB2 is indeed expressed in KI mice.

Susceptibility of hSCARB2 KI mice to EV71 infection. To assess the susceptibility of hSCARB2 KI mice to EV71 infection, we inoculated 5-, 7-, 10-, 14-, and 21-day-old and adult KI and WT mice intracerebrally (i.c.), intramuscularly (i.m.), and intraperitoneally (i.p.) with EV71 (2×10^6 PFU) and observed them for the development of clinical signs. The WT and KI mice which were inoculated i.c., i.m., or i.p. with EV71 showed a reduction in survival rate (Fig. 3A to C; Fig. 3G to I; also, see Table S3 in the supplemental material). Relative to WT mice, lower survival rates were observed in KI mice. After EV71 infection via different routes, WT and KI mice at the indicated ages showed ataxia, limb paralysis, and death (Fig. 3D to F; Fig. 3J and L; also, see Table S3). However, the incidence of the above neurological symptoms in KI mice was much higher than that in WT mice. KI mice were susceptible to infection via the i.c. route.

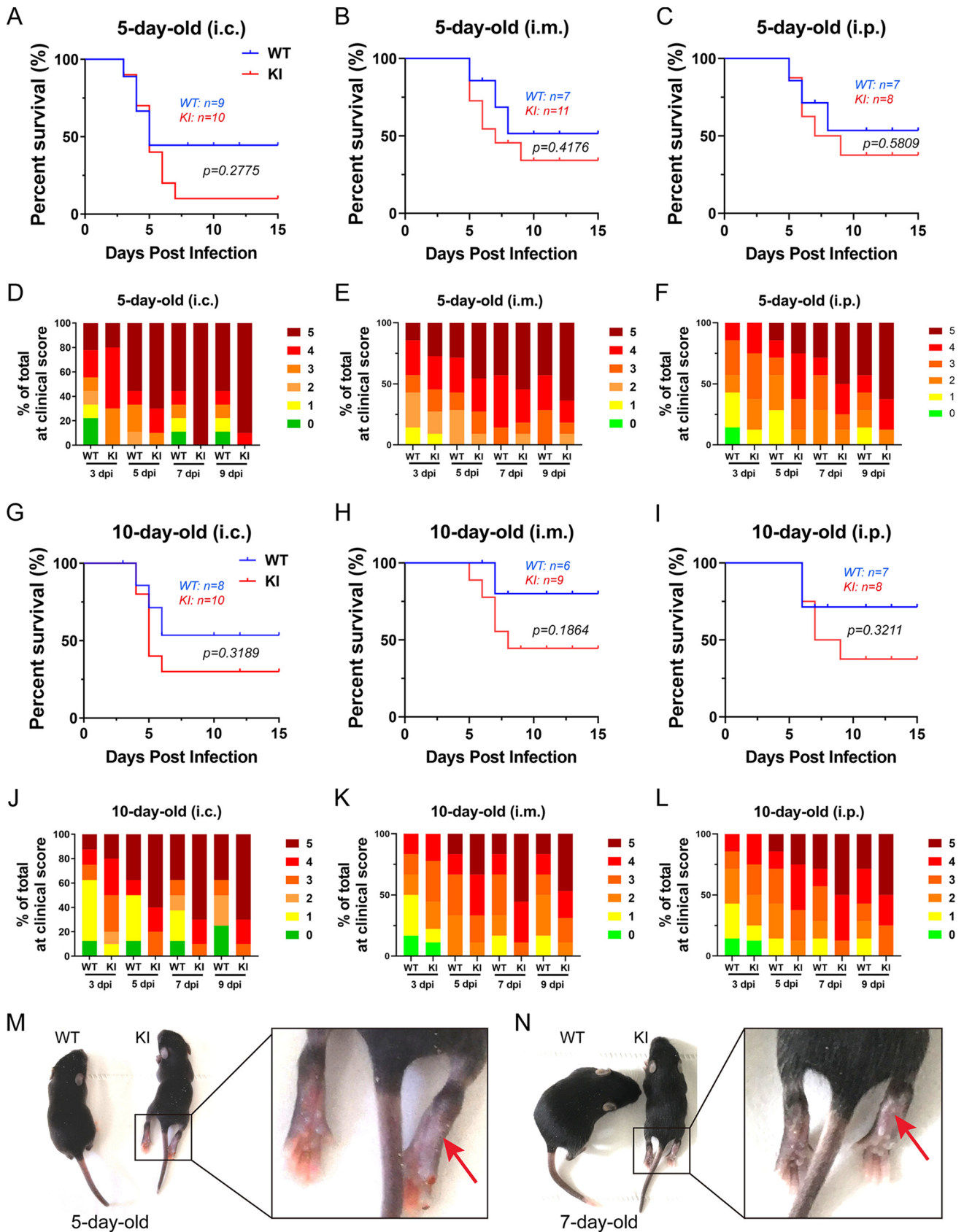


FIG 3 The susceptibility of hSCARB2 KI mice to EV71 infection. (A to C) Five-day-old WT and KI mice were infected with EV71 by different routes (i.c. [A], i.p. [B], and i.m. [C]). (D to F) Clinical scores of WT and KI mice after EV71 infection at indicated times. 0, healthy; 1, reduced mobility; 2, ruffled fur and (Continued on next page)

Under the conditions of i.m. and i.p. inoculation (Fig. 3H and I; Fig. 3K and L; Table S3), WT mice were resistant to EV71 infection. Figure 3M and N show hind limb paralysis and weight loss in 5- and 7-day-old KI mice after EV71 infection. The above results indicated that hSCARB2 KI mice were more likely to develop neurological symptoms and exhibited age-dependent changes in their susceptibility to EV71.

Histopathological examination of EV71-infected mice. Histopathological examinations of 10-day-old WT and KI mice at 7 days postinfection (dpi) were performed (Fig. 4). Brain tissues and spinal cord presented focal, moderate to severe neural degeneration and gliosis in KI mice at 7 dpi; brain tissues and spinal cords from WT mice displayed focal, minimal to slight changes. Skeletal muscle exhibited severe necrotizing myositis with fragmentation of myofibers and inflammatory cell infiltration in the limbs of KI mice at 7 dpi, but equivalent tissues in WT mice were only slightly affected. No obvious pathological changes were found in myocardial tissues from WT and KI mice. Large areas of hyperemia and necrosis-like lesions in liver tissues of KI mice were found at 7 dpi; only hyperemia in liver tissues was observed in WT mice. Spleen tissues from KI mice showed severe hyperemia and cavitation at 7 dpi, whereas spleen tissues in WT mice displayed these histopathological features to a mild degree. We also observed the rupture of the small intestine villi and vacuolation of the basement membrane in KI mice at 7 dpi, but equivalent tissues in WT mice exhibited only slight changes. Together, our data suggested that that EV71 could induce severe pathological changes in the CNS and skeletal muscle of hSCARB2 KI mice.

Pathology and apoptosis in EV71-infected lungs. Because cardiopulmonary failure is responsible for the death in severe EV71 infections, we focused our subsequent studies on lung pathological changes. The images of lungs from 10-day-old KI mice presented more severe hyperemia at 5 and 7 dpi (Fig. 5A). Through hematoxylin-and-eosin (H&E) staining (Fig. 5A), we did not observe leukocyte infiltration, but vascular leakage and alveoli filled with erythrocytes were noted, suggesting edema and hemorrhage in EV71-infected KI mice. However, WT mice displayed slight to mild changes in these histopathological features. We detected neither inflammation nor hyperemia in the lungs of uninfected control mice. Immunofluorescence microscopy revealed that the number of TUNEL (terminal deoxynucleotidyltransferase-mediated dUTP-biotin nick end labeling)-positive (apoptotic) cells in lung sections from KI mice was greatly increased over that in WT mice at 5 and 7 dpi (Fig. 5B and C). Quantitative results showed that the pathological score (Fig. 5D) and number of TUNEL-positive (apoptotic) cells (Fig. 5E) in EV71-infected KI mice were higher than those in WT mice at 5 and 7 dpi. Together, our results suggested that EV71 infection caused severe lung damage in hSCARB2 KI mice.

Viral replication and activation of glial cells in EV71-infected brains. EV71 infections are often accompanied by neurological complications. To further evaluate the extent of CNS lesions in EV71-infected mice, we detected viral replication and glial cells in brain sections. Through immunofluorescence double staining, we observed colocalization between EV71 and caspase-3 (Fig. 6A), EV71 and NeuN-labeled neurons (Fig. 6B), EV71 and GFAP (glial fibrillary acidic protein)-labeled astrocytes (Fig. 6C), and EV71 and IBA-1 (ionized calcium-binding adaptor molecule 1)-labeled microglial cells (Fig. 6D). The number of EV71⁺ caspase-3⁺ (Fig. 6E), EV71⁺ NeuN⁺ (Fig. 6F), and EV71⁺ GFAP⁺ (Fig. 6G) cells in EV71-infected brain tissue from KI mice was higher than that in WT mice at 5 and 7 dpi, indicating the sensitivity of KI mice to EV71 in the CNS. EV71 mainly infected astrocytes and replicated in only a limited number of neurons and microglial cells (Fig. 6H). The number of astrocytes (Fig. 6I) and microglial cells (Fig. 6J) in EV71-infected brains from KI mice was higher than that in WT mice, suggesting

FIG 3 Legend (Continued)

hunched back; 3, ataxia and weight loss; 4, limb weakness; and 5, dying or death. (G to I) Ten-day-old WT and KI mice were infected with EV71 by different routes (i.e. [G], i.p. [H], and i.m. [I]). (J to L) Clinical scores of WT and KI mice after EV71 infection at the indicated times. The log-rank test was used to analyze the statistical difference of the survival rate of EV71-infected KI versus WT mice. (M and N) Clinical signs of 5- and 7-day-old KI mice after EV71 infection. *n*, number of mice per group.

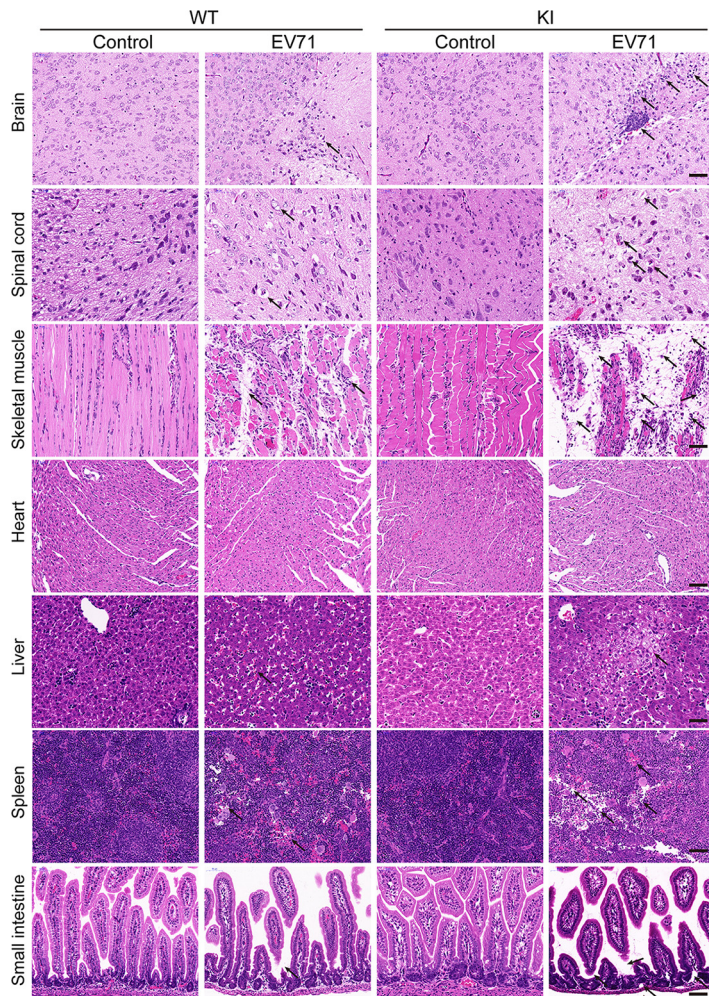


FIG 4 Histopathological examination of EV71-infected mice. Ten-day-old WT and KI mice were infected via i.p. injection of EV71 at 2×10^6 PFU. The animals were euthanized at 7 dpi, and paraffin-embedded tissue sections of the organs were stained with H&E. The specimens are representatives of 5 to 7 mice in each group, with similar histology. The tissue damage (arrows) was assessed by a pathologist. Bars = $50 \mu\text{m}$.

more severe CNS damage in KI mice. Together, our data indicated that hSCARB2 KI mice were more sensitive to CNS damage caused by EV71 infection. It is possible that the increased number of astrocytes and microglial cells might play a critical role in CNS pathogenesis.

Leukocytes in the brains of EV71-infected KI mice. To characterize CNS inflammation, we examined the changes of immune cells in brain slices. Ten-day-old KI mice were inoculated i.p. with the virus or RD cells, and the brains were harvested at 3, 5, and 7 dpi. Leukocyte infiltration was visualized by staining with anti-CD45 antibody, and T cells, neutrophils, and monocytes/macrophages were detected by colocalization of CD45 with CD3 (Fig. 6A), Ly6G (Fig. 7C), and CD11b (Fig. 7E), respectively. Only very small numbers of T cells (Fig. 7B) and neutrophils (Fig. 7D) were detected in the brain slices from KI mice after EV71 infection, but the number of monocytes/macrophages was significantly increased around the blood-brain barrier at 3, 5, and 7 dpi. Our results suggest that the increased number of monocytes/macrophages is a feature of CNS inflammation induced by EV71 infection.

Cytokines in the serum of EV71-infected KI mice. Cytokine release plays an important role in EV71 pathogenesis. We evaluated the changes in the production of cytokines in the serum of EV71-infected KI mice. Ten-day-old KI mice were inoculated

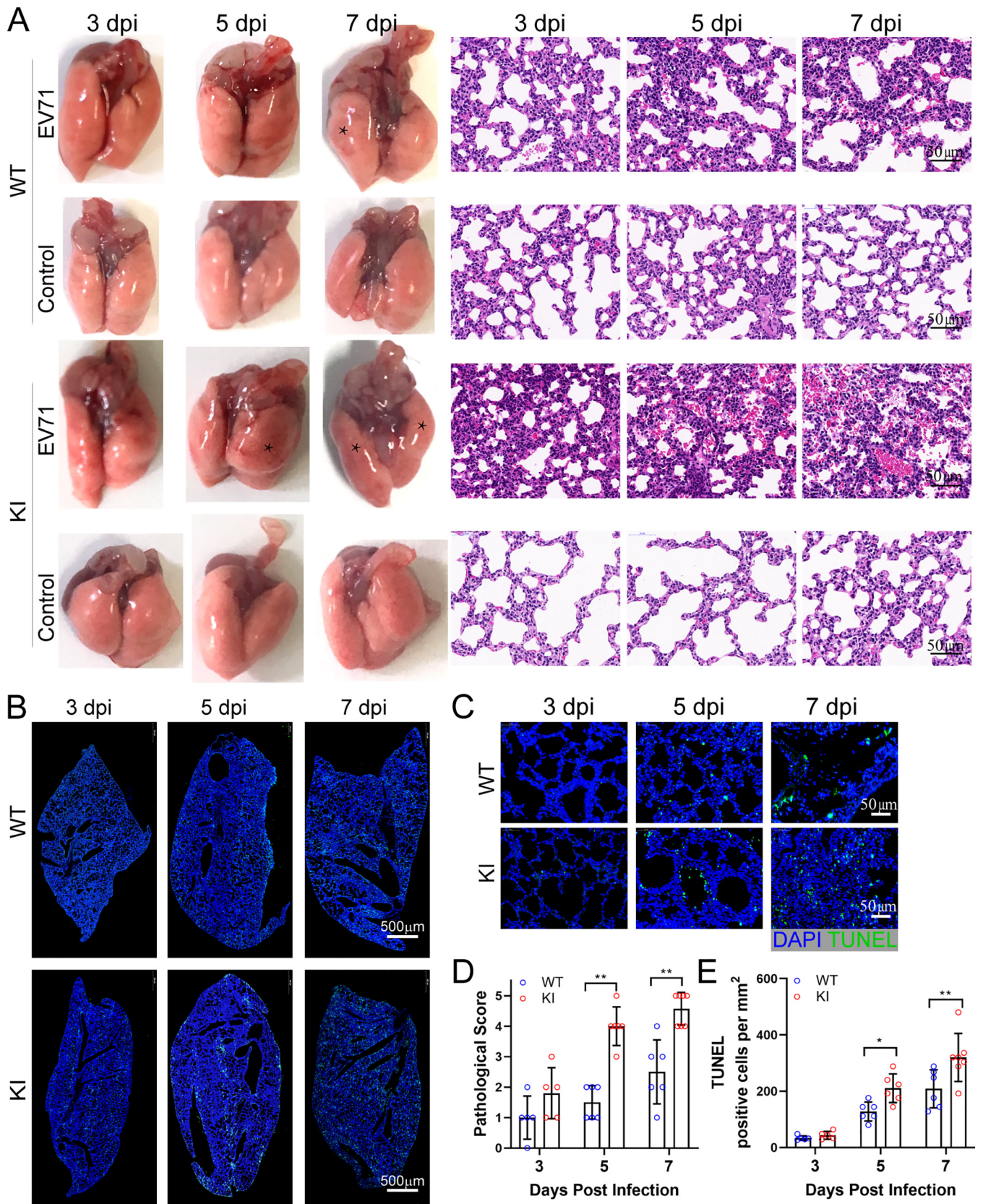


FIG 5 Pathology and apoptosis in EV71-infected lungs. Ten-day-old WT and KI mice were infected via i.p. injection of EV71 at 2×10^6 PFU. The animals were euthanized at 3, 5, and 7 dpi, and lung tissues were removed (A). Stars indicate pulmonary congestion. Paraffin-embedded tissue sections of the lungs (Continued on next page)

i.p. with the virus or RD cells, and blood was collected from the hearts at 1, 3, 5, and 7 dpi. A cytokine array was used to determine the relative levels of secreted cytokines and chemokines. From the 40 cytokines included in the array, we detected only eight cytokines in the serum of EV71-infected mice (Fig. 8A). Among them, the release of complement 5 (C5)/C5a (Fig. 8B), interferon gamma-induced protein-10 (IP-10) (Fig. 8D), and chemokine (C-X-C motif) ligand 9 (CXCL9) (Fig. 8E) was much increased by EV71 infection. In addition, the release of soluble intercellular cell adhesion molecule-1 (sICAM-1) (Fig. 8C), granulocyte–macrophage colony-stimulating factor (GM-CSF) (Fig. 8F), monocyte chemoattractant protein 1 (MCP-1) (Fig. 8G), CXCL12 (Fig. 8H), and tissue inhibitor of metalloproteinase 1 (TIMP-1) (Fig. 8I) was also enhanced. These findings suggested that EV71 infection induced the release of proinflammatory cytokines into the serum of hSCARB2 KI mice.

DISCUSSION

SCARB2 and P-selectin glycoprotein ligand 1 (PSGL-1) are human transmembrane proteins which have been identified as functional receptors for the entry of EV71 (13, 26). PSGL-1 is a key factor involved in early inflammatory events on immune cells. Transfection of mouse L929 cells with PSGL-1 enables EV71 entry and replication, as well as the development of cytopathic effects. However, only a limited number of EV71 strains can use PSGL-1 as a receptor to enter cells (26), and the human PSGL-1 transgene does not enhance the infectivity of clinical EV71 strains in mice (20). Unlike PSGL-1, SCARB2 can be used by most EV71 strains as an entry receptor in nonsusceptible mouse cells, suggesting that SCARB2 plays a crucial role in supporting viral infection (13, 26). BAC-mediated hSCARB2 transgenic mice or chimeric mSCARB2/hSCARB2 mice were previously used for EV71 study and developed neurological symptoms strikingly resembling infection in humans (21, 22). Here, we generated a novel *Rosa26*-targeted hSCARB2 KI mouse model via the CRISPR/Cas9 system. We demonstrated that the exogenous expression of hSCARB2 in mice conferred susceptibility to EV71 infection. The infected KI mice displayed neurological and respiratory symptoms similar to severe cases of human infection, which should be useful for studying the neuropathogenesis and lung damage induced by EV71.

EV71 is considered a type of neurotropic virus (27). Inflammation and EV71 antigens are detected mainly in the brain stem, spinal cord, hypothalamus, and cerebellar dentate nuclei in fatal human encephalomyelitis (28). In the past decade, epidemiological studies and relevant clinical reports have suggested that the CNS is the major target of EV71 infection (2, 3, 29). EV71 can cause different neurological manifestations in humans, such as encephalomyelitis, polio-like acute flaccid paralysis, and meningitis (2). In primate models, neurological manifestations were observed after EV71 inoculation via i.c., intravenous (i.v.), respiratory, or digestive routes. Histopathological examinations confirmed viral replication in the spinal cord, brain stem, cerebellar dentate nuclei, and cerebrum (7, 30). In comparison, hSCARB2 KI mice infected with EV71 via the i.c., i.v., or i.p. route demonstrated paralysis, ataxia, and severe lesions. EV71 antigens were detected in the brain stem, spinal cord, skeletal muscle, and lungs of most animals. Additionally, EV71 mainly infected astrocytes. Only a limited number of neurons and microglial cells were affected. Our investigations highlighted the similarities of EV71 neurotropism observed in human patients, monkeys, and transgenic mice (7, 22, 28–30).

Young age at disease onset is associated with increased risk of HFMD severity (31). Likewise, animal age also appears to be related to viral susceptibility. Up to the age of 2 weeks, KI mice were susceptible to EV71 infection via the i.c., i.p. or i.m. route. Previously, transgenic mice had also displayed a susceptibility to viral inoculation via the i.v. and i.p. routes up to the age of 2 weeks (21, 22, 32). These findings imply the presence of host factors that limit infection through antiviral immunity. However,

FIG 5 Legend (Continued)

were stained with H&E (A) and TUNEL (B and C). The specimens are representative of 5 to 7 mice in each group. Pathological score (D) was determined by a pathologist, and the number of TUNEL-positive cells (E) per slice was quantified with ImageJ software. Bar = 500 (B) and 50 (C) μ m. (D and E) *, $P < 0.05$ versus WT; **, $P < 0.01$ versus WT.

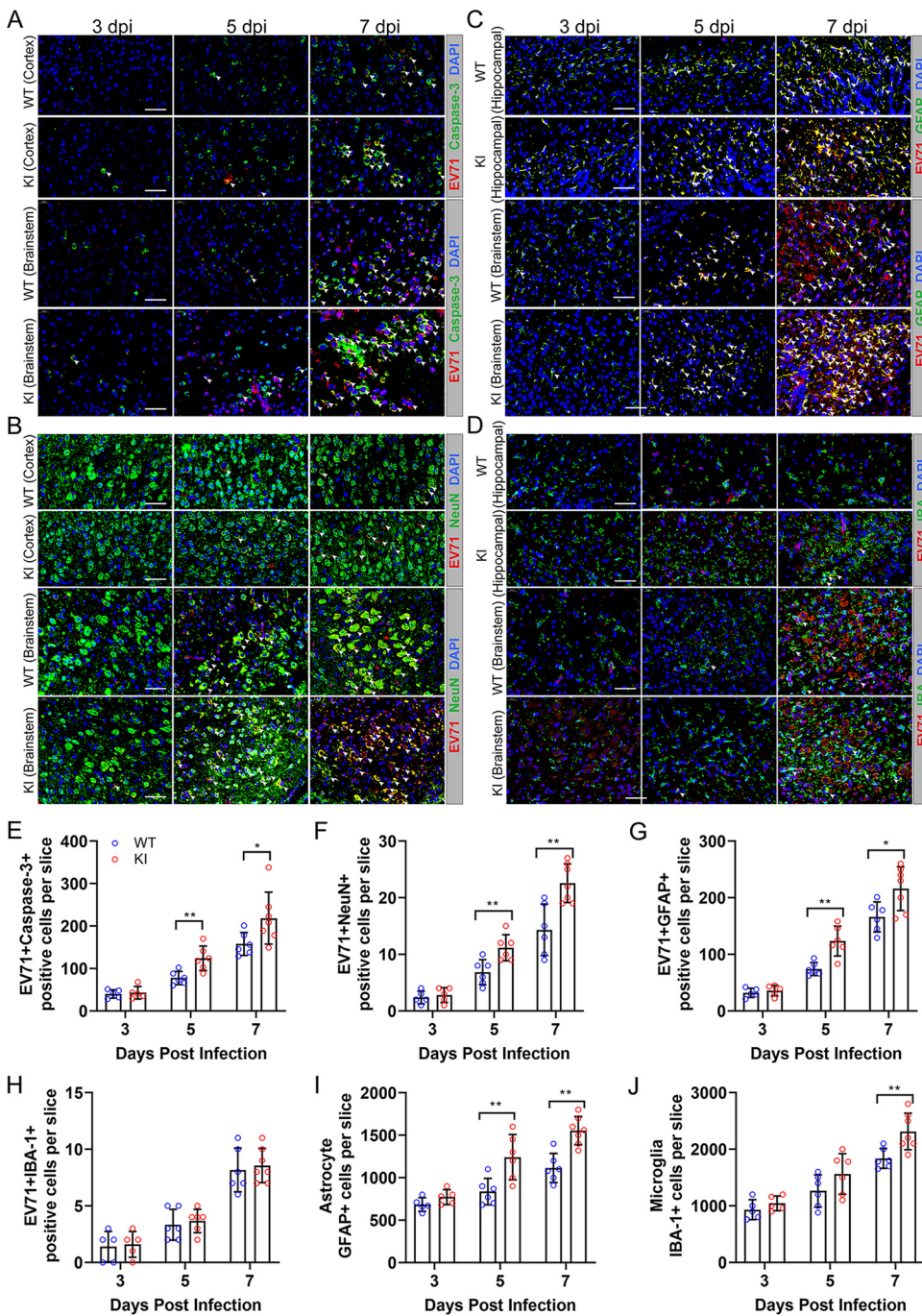


FIG 6 Viral replication and activation of glial cells in EV71-infected brains. Ten-day-old WT and KI mice were infected via i.p. injection of EV71 at 2×10^6 PFU. The animals were euthanized at 3, 5, and 7 dpi, and brain tissues were removed. Paraffin-embedded tissue sections of the brains were stained to evaluate the virus antigen/apoptotic cells (A), neurons (B), astrocytes (C), and microglial cells (D). Bars = $50 \mu\text{m}$. The number of EV71+ caspase-3+ cells (E), EV71+ NeuN+ cells (F), EV71+ GFAP+ cells (G), EV71+ IBA-1+ cells (H), astrocytes (I), and microglial cells (J) per slice was quantified using ImageJ software. *, $P < 0.05$ versus WT; **, $P < 0.01$ versus WT.

immunodeficient mice, for example, AG129 mice and NOD/SCID mice, also exhibited age-dependent changes in their susceptibility to EV71 (33). Which host factors determine viral susceptibility remains to be investigated.

Several differences were observed between KI mice and previously described transgenic mice. Our hSCARB2 KI mice were less susceptible to oral infection and did not display the typical skin lesions found in human infections (3). Yang et al. introduced a

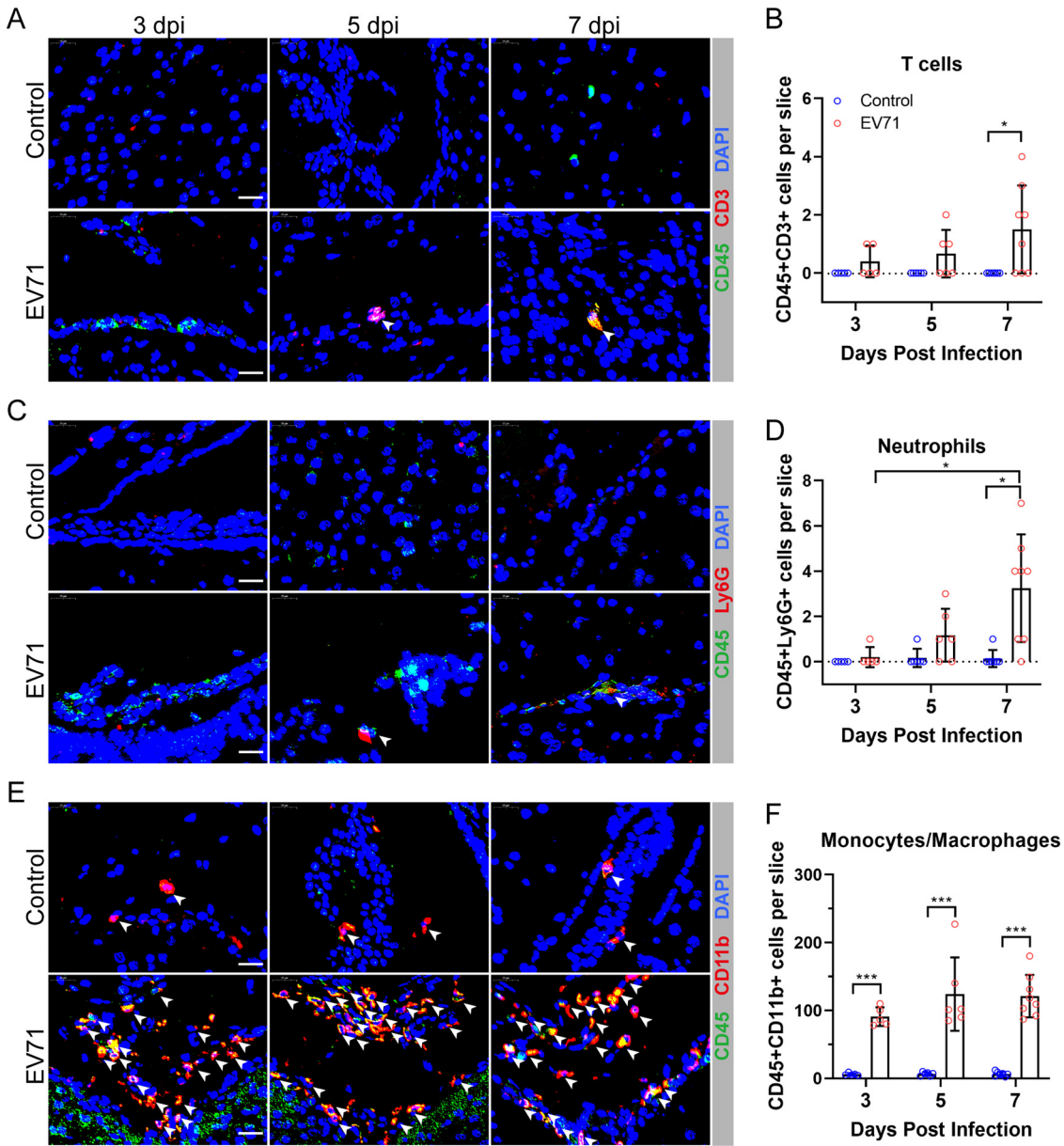


FIG 7 Leukocytes in the brains of EV71-infected KI mice. Ten-day-old KI mice were infected via i.p. injection of EV71 at 2×10^6 PFU. The animals were euthanized at 3, 5, and 7 dpi, and brain tissues were removed. Paraffin-embedded tissue sections of the brains were stained to evaluate T cells (A), neutrophils (C), and monocytes/macrophages (E). Bars = $20 \mu\text{m}$. The number of CD45⁺ CD3⁺ cells (B), CD45⁺ Ly6G⁺ cells (D), and CD45⁺ CD11b⁺ cells (F) per slice was quantified with ImageJ software. *, $P < 0.05$ versus control; **, $P < 0.01$ versus control; ***, $P < 0.001$ versus control.

chimeric mSCARB2/hSCARB2 mouse model that was highly susceptible to oral infection (22). Compared with the minor damage in the skeletal muscle of mSCARB2/hSCARB2 chimeric mice (22), severe lesions such as myolysis and necrosis were found in EV71-infected KI mice. In fact, high viral titers and severe pathological changes in skeletal muscle were observed in EV71-infected mouse models (8, 9, 12, 34). EV71 has been suggested to replicate primarily in skeletal muscle and causes severe necrotizing myositis, which further leads to respiratory failure due to necrotizing myositis of respiratory-related muscles (35). Pulmonary hemorrhage and edema, which have been reported to be one of the fatal outcomes of human infections (36–38), were also observed in our KI mouse model. The histopathology of the lung from a fatal case showed marked edema and hemorrhage with mild pneumonic changes (37), which was detected in EV71-infected KI mice. Relative to WT mice, KI mice were more likely

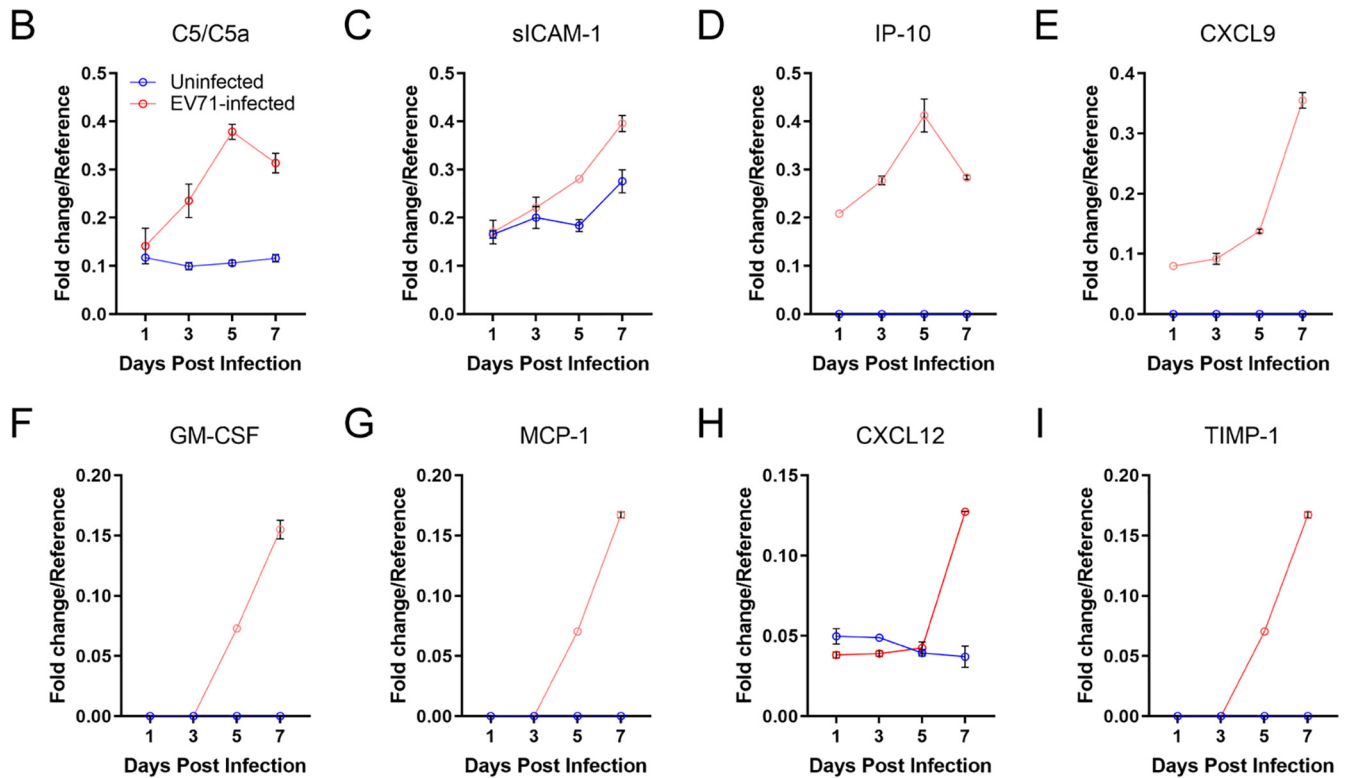
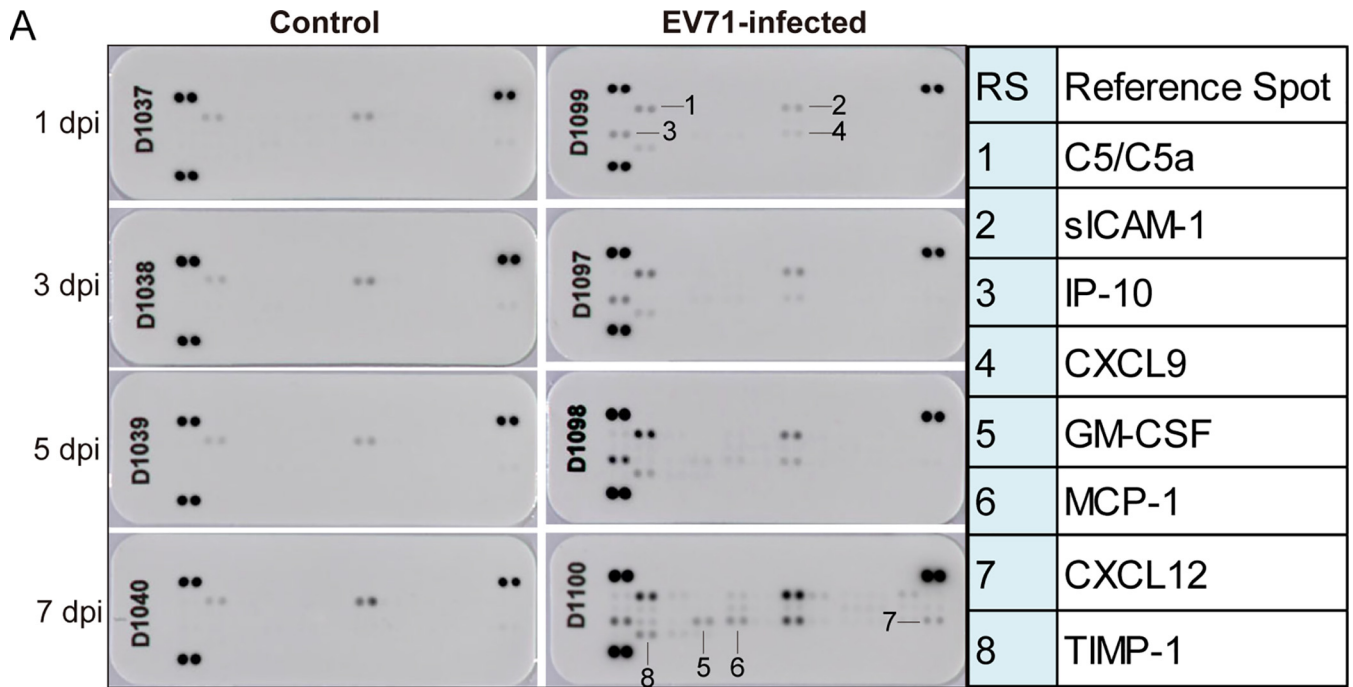


FIG 8 Cytokines in the serum of EV71-infected KI mice. Ten-day-old KI mice were infected via i.p. injection of EV71 at 2×10^6 PFU. The animals were euthanized at 1, 3, 5, and 7 dpi, and blood was collected from the heart. A mouse array analysis (A) was used to detect the relative levels of 40 cytokines in the serum of mice. The release of C5/C5a (B), sICAM-1 (C), IP-10 (D), CXCL9 (E), GM-CSF (F), MCP-1 (G), CXCL12 (H), and TIMP-1 (I) was quantified with ImageJ software. The results are representative of two mice in each group.

to develop pulmonary hemorrhage and edema following EV71 infection. Compared with other hSCARB2 transgenic mouse models, which did not display the typical lung damage found in human infections (21, 22, 32), our KI mouse model can be used to study lung pathogenesis caused by EV71 infection.

Glial cells, such as astrocytes and microglia, play pivotal roles in the CNS response to insults, whether physical, infectious, or neurodegenerative disease related (39). Generally, the hallmark of these conditions is neuroinflammation, characterized by activation of glial cells and production of pro- and/or anti-inflammatory cytokines and chemokines (39). After EV71 infection, the numbers of astrocytes and microglia were increased significantly in the brains from WT and KI mice, and EV71-infected KI mice had more glial cells, suggesting the presence of severe lesions in KI mice. Our results were in agreement with previous studies that show astrocyte and microglial activation in the brains of EV71-infected mice (22, 40). Necropsy showed edema with an increase in microglia and astrocytic proliferation in the cerebral tissue, but no lymphocytic infiltration was evident (37). In our study, in addition to the increase in monocytes/macrophages around the blood-brain barrier, we did not observe massive leukocyte infiltration, and only a limited number of T cells and neutrophils were found in EV71-infected KI brains. Therefore, our KI mice are suitable for the study of the pathogenesis of CNS lesions induced by EV71.

Cytokines play a significant role in the development of HFMD (41, 42). We examined the cytokine release in the serum of EV71-infected KI mice. Of note, C5/C5a was increased in response to EV71. Complement is a complex innate immune surveillance system, acting as the first line of defense against pathogens (43). The fragment of C5/C5a is an inflammation mediator which can induce local inflammation and cause tissue damage (43). Targeted complement inhibition has been considered as a potential therapeutic strategy for the inflammatory response induced by EV71 (44). IP-10 and CXCL9 are mainly generated from monocytes/macrophages and astrocytes upon infection (45). GM-CSF and MCP-1 are mainly secreted by most leukocytes (46). sICAM-1 is released by endothelial cells upon dysfunction, which is best known for regulating leukocyte recruitment from the circulation to sites of inflammation (47). The increase of IP-10, CXCL9, GM-CSF, MCP-1, sICAM-1, CXCL12, and TIMP-1 can recruit different leukocyte subsets and further lead to local inflammation. Plasma levels of IP-10, GM-CSF, and MCP-1 were significantly elevated in HFMD patients (42). In our previous study, we found that the expression of ICAM-1 was increased in EV71-infected lungs (34). Collectively, our study suggested that hSCARB2 KI mice can be used to study the immunopathogenesis of EV71.

In summary, we generated a novel *Rosa26*-targeted hSCARB2 KI mouse model via the CRISPR/Cas9 system. This murine model not only displayed neurological complications similar to human infections but also developed a respiratory syndrome. Thus, our mouse model is suitable for the study of EV71 pathogenesis. In addition, this murine model can be used to develop antiviral therapeutics and evaluate the efficacies of EV71 vaccines in the future.

MATERIALS AND METHODS

Ethics statement. Experiments using genome editing and pathogens were reviewed and approved by the Life Science Ethics Review Committee of Zhengzhou University, and the experiments were performed strictly in accordance with the guidelines of Zhengzhou University for animal experiments. All human histological samples used in this study were obtained ethically, and the protocols were approved by the relevant ethics committee of Zhengzhou University.

Cells and viruses. Human rhabdomyoma (RD) cells and African green monkey kidney (Vero) cells (ATCC CCL-81) were cultured in DMEM (Gibco, New York, NY, USA) supplemented with 10% fetal bovine serum (FBS) (Gibco, New York, USA). As described previously, EV71 strain ZZ1350 (GenBank no. [KY886010](#)) was isolated from a nonfatal case with CNS involvement in Children's Hospital of Zhengzhou (Zhengzhou, Henan, China) (9).

Virus enrichment and titration. Approximately 1×10^7 RD cells cultured in 3 ml 2% (vol/vol) FBS-Dulbecco's modified Eagle medium (DMEM) were infected with EV71 at a multiplicity of infection of 0.01. The cells and medium were frozen at 72 h after infection. After thawing, the cell debris was removed by centrifugation at $10,000 \times g$ for 20 min at room temperature. Subsequently, the supernatant was filtrated with a 0.22- μ m filter. The viral titers were determined by plaque assay using RD cells (12). Working stocks (10^8 PFU per ml) were stored at -80°C .

Mice. C57BL/6N and ICR mice used in this study were purchased from Beijing Vital River Laboratory Animal Technology Co., Ltd., and all mice were housed in individually ventilated cages (IVC; Fengshi Group) in a specific-pathogen-free facility at the College of Public Health of Zhengzhou University; animals were on a 12-h light/dark cycle with *ad libitum* access to food and water.

Generation of *Rosa26*-targeted *hSCARB2* KI F0 mice via CRISPR/Cas9 in C57BL/6 zygotes. The single-guide RNAs (sgRNAs) were designed using online software (<http://crispor.tefor.net/>). Two specific allele sites were selected as target sequences in introns 1 and 2 of the mouse *Rosa26* locus. The two target sequences were sgRNA1 (5'-GAAGATGGCGGGAGTCTTCTGG-3') and sgRNA2 (5'-CGCCCATCTTCTAGAAAGACTGG-3'). The sgRNAs and Cas9 mRNA were produced by *in vitro* transcription (IVT) as described previously (24). The targeting donor DNA was synthesized (GenScript Biotechnology) containing homology arms for homologous recombination and *hSCARB2* (GenBank no. [NM_005506](#)) expression elements. The target fragment and pUC57Kan-R26 vector were linked by homologous recombination (Fig. S1). Four-week-old female C57BL/6N mice were intraperitoneally (i.p.) injected with pregnant mare serum gonadotropin followed by human chorionic gonadotropin (10 U/mouse) 48 h later and then mated with 12-week-old C57BL/6N male mice immediately. Fertilized embryos were collected the next morning, and Cas9 mRNA (50 ng/ml), sgRNA (50 ng/ml), and *hSCARB2*-targeting construct (10 ng/ml) were microinjected into the cytoplasm of fertilized embryos by using a standard microinjection system (TransferMan 4r; Eppendorf, Germany). Surviving eggs were cultured at 37°C in 5% CO₂ overnight, and on the next day, they were transferred into the oviducts of pseudopregnant ICR mice to obtain live pups. The resulting mice were screened by PCR analysis using PCR primer sets (Table S1) for the *hSCARB2* gene, and genomic DNA extracted from tail biopsy specimens was used as a template. The expression of *hSCARB2* mRNA in the different organs and tissues from wild-type (WT) and KI mice and positive-control (PC) human RD cells was measured by quantitative real-time PCR. The sample without template (ddH₂O) was regarded as a negative control.

EV71 infection in mice. WT or KI mice (5, 7, 10, 14, and 21 days old or adult) were infected with the viruses (2×10^6 PFU) or RD cell supernatant via intracranial (i.c.), intraperitoneal (i.p.), or intramuscular (i.m.) inoculation and were observed for clinical signs. Control-infected mice were injected with the same volume of RD cell culture supernatants. Clinical scores were defined as follows: 0, healthy; 1, reduced mobility; 2, ruffled fur and hunched back; 3, ataxia and weight loss; 4, limb weakness; and 5, dying or death. Blood was collected from the heart, and the organs and tissues were removed from euthanized mice at the indicated time points and fixed with 4% paraformaldehyde at 4°C for 48 h. After fixation, the organs and tissues were subjected to histopathological and immunohistochemical (IHC) analysis.

Histopathological and IHC analysis. After fixation, paraffin-embedded organs and tissues were cut into 5- μ m sections and stained with hematoxylin and eosin (H&E). The expression of *hSCARB2* in the organs and tissues was detected by a standard immunoperoxidase procedure, as described previously (48).

Immunofluorescence staining. Paraffin-embedded sections were stained to evaluate the virus antigen/apoptotic cells (TUNEL staining or labeling with caspase-3), neurons (labeled with NeuN), glial cells (microglia labeled with IBA-1; astrocytes labeled with GFAP), T cells (labeled with CD45 and CD3), neutrophils (labeled with CD45 and Ly6G), and monocytes/macrophages (labeled with CD45 and CD11b). Immunofluorescence staining and scanning technical service were provided by Servicebio Biotech Co., Ltd. The number of positively staining cells per slice was quantified with ImageJ software.

Antibodies. The following primary antibodies were used in this study: goat anti-human *SCARB2* antibody (R&D Systems; catalog no. AF1966), mouse anti-EV71 antibody (GeneTex, Inc.; catalog no. GTX41306). Rabbit anti-IBA-1 antibody (catalog no. GB13105-1), NeuN antibody (catalog no. GB11138), and caspase-3 antibody (catalog no. GB11138) were from Servicebio Biotech. Rabbit anti-CD3 antibody (catalog no. ab133357), GFAP antibody (catalog no. ab7260), Ly6G antibody (catalog no. ab25377), rat anti-CD45 antibody (catalog no. ab25386), and mouse anti-CD45 antibody (catalog no. ab33923) were from Abcam, Inc.

BMM ϕ culture. Macrophages (BMM ϕ) used in this study were derived from the bone marrow cells of WT C57BL/6J and KI mice. BMM ϕ were cultured in RPMI 1640 supplemented with 20% L929 cell culture medium and 10% FBS for ~4 to 9 days, and then adherent cells were harvested for Western blot analysis.

Western blot analysis. Total proteins from the organs and tissues of mice and RD cells were extracted with a protein extraction kit (CWbio Company Ltd.) based on the manufacturer's instructions. For Western blot analysis, samples were separated by SDS-PAGE and transferred to polyvinylidene difluoride (PVDF) membranes. After incubation with primary antibodies, PVDF membranes were washed three times and incubated with anti-goat secondary antibodies. Finally, membranes were washed three times and developed with an enhanced chemiluminescence kit (Absin Bioscience, Inc.).

Cytokines. R&D Systems mouse cytokine array panel A (catalog no. ARY006) was used to detect the relative levels of 40 cytokines in the serum (70 μ l/mouse) of control and EV71-infected mice. The results were quantified with ImageJ software.

Statistical analysis. Statistical analysis was performed with GraphPad Prism version 8.3 (GraphPad 8.3 Software, San Diego, CA, USA). The Mantel-Cox log rank test was used to compare the survival of different group mice. The results were expressed as the mean \pm standard deviation (SD). Differences in the pathological score and positive-stained cell numbers were assessed using unpaired Student *t* test or one-way analysis of variance (ANOVA). A *P* value of < 0.05 after two-tailed *t* testing was regarded as significant.

SUPPLEMENTAL MATERIAL

Supplemental material is available online only.

FIG S1, TIF file, 0.6 MB.

TABLE S1, DOCX file, 0.01 MB.

TABLE S2, DOCX file, 0.02 MB.

TABLE S3, DOCX file, 0.02 MB.

ACKNOWLEDGMENTS

We thank the Centre d'Immunologie de Marseille-Luminy (Aix Marseille Université, INSERM, CNRS, Marseille, France) for providing pUC57Kan-R26 vector.

This work was supported by the National Natural Science Foundation of China (82002147 and 82073618), the Project founded by China Postdoctoral Science Foundation (2019M662543), and Key Scientific Research Project of Henan Institution of Higher Education (21A310026). The mouse genetic engineering platform in Xinxiang Medical University is sponsored by the 111 Project (D20036).

We declare no conflict of interest.

REFERENCES

- Schmidt NJ, Lennette EH, Ho HH. 1974. An apparently new enterovirus isolated from patients with disease of the central nervous system. *J Infect Dis* 129:304–309. <https://doi.org/10.1093/infdis/129.3.304>.
- Solomon T, Lewthwaite P, Perera D, Cardoso MJ, McMinn P, Ooi MH. 2010. Virology, epidemiology, pathogenesis, and control of enterovirus 71. *Lancet Infect Dis* 10:778–790. [https://doi.org/10.1016/S1473-3099\(10\)70194-8](https://doi.org/10.1016/S1473-3099(10)70194-8).
- Ho M, Chen ER, Hsu KH, Twu SJ, Chen KT, Tsai SF, Wang JR, Shih SR. 1999. An epidemic of enterovirus 71 infection in Taiwan. Taiwan Enterovirus Epidemic Working Group. *N Engl J Med* 341:929–935. <https://doi.org/10.1056/NEJM199909233411301>.
- Chan LG, Parashar UD, Lye MS, Ong FG, Zaki SR, Alexander JP, Ho KK, Han LL, Pallansch MA, Suleiman AB, Jegathesan M, Anderson LJ, Outbreak Study Group. 2000. Deaths of children during an outbreak of hand, foot, and mouth disease in sarawak, malaysia: clinical and pathological characteristics of the disease. *Clin Infect Dis* 31:678–683. <https://doi.org/10.1086/314032>.
- Chang LY, Lin TY, Hsu KH, Huang YC, Lin KL, Hsueh C, Shih SR, Ning HC, Hwang MS, Wang HS, Lee CY. 1999. Clinical features and risk factors of pulmonary oedema after enterovirus-71-related hand, foot, and mouth disease. *Lancet* 354:1682–1686. [https://doi.org/10.1016/S0140-6736\(99\)04434-7](https://doi.org/10.1016/S0140-6736(99)04434-7).
- Nagata N, Iwasaki T, Ami Y, Tano Y, Harashima A, Suzuki Y, Sato Y, Hasegawa H, Sata T, Miyamura T, Shimizu H. 2004. Differential localization of neurons susceptible to enterovirus 71 and poliovirus type 1 in the central nervous system of cynomolgus monkeys after intravenous inoculation. *J Gen Virol* 85:2981–2989. <https://doi.org/10.1099/vir.0.79883-0>.
- Zhang Y, Cui W, Liu L, Wang J, Zhao H, Liao Y, Na R, Dong C, Wang L, Xie Z, Gao J, Cui P, Zhang X, Li Q. 2011. Pathogenesis study of enterovirus 71 infection in rhesus monkeys. *Lab Invest* 91:1337–1350. <https://doi.org/10.1038/labinvest.2011.82>.
- Khong WX, Yan B, Yeo H, Tan EL, Lee JJ, Ng JK, Chow VT, Alonso S. 2012. A non-mouse-adapted enterovirus 71 (EV71) strain exhibits neurotropism, causing neurological manifestations in a novel mouse model of EV71 infection. *J Virol* 86:2121–2131. <https://doi.org/10.1128/JVI.06103-11>.
- Jin Y, Zhang C, Zhang R, Ren J, Chen S, Sui M, Zhou G, Dang D, Zhu J, Feng H, Xi Y, Yang H, Duan G. 2017. Pulmonary edema following central nervous system lesions induced by a non-mouse-adapted EV71 strain in neonatal BALB/c mice. *Virol J* 14:243. <https://doi.org/10.1186/s12985-017-0911-5>.
- Shih C, Liao CC, Chang YS, Wu SY, Chang CS, Liou AT. 2018. Immunocompetent and immunodeficient mouse models for enterovirus 71 pathogenesis and therapy. *Viruses* 10:674. <https://doi.org/10.3390/v10120674>.
- Wang W, Duo J, Liu J, Ma C, Zhang L, Wei Q, Qin C. 2011. A mouse muscle-adapted enterovirus 71 strain with increased virulence in mice. *Microbes Infect* 13:862–870. <https://doi.org/10.1016/j.micinf.2011.04.004>.
- Wang YF, Chou CT, Lei HY, Liu CC, Wang SM, Yan JJ, Su LJ, Wang JR, Yeh TM, Chen SH, Yu CK. 2004. A mouse-adapted enterovirus 71 strain causes neurological disease in mice after oral infection. *J Virol* 78:7916–7924. <https://doi.org/10.1128/JVI.78.15.7916-7924.2004>.
- Yamayoshi S, Yamashita Y, Li J, Hanagata N, Minowa T, Takemura T, Koike S. 2009. Scavenger receptor B2 is a cellular receptor for enterovirus 71. *Nat Med* 15:798–801. <https://doi.org/10.1038/nm.1992>.
- Kuronita T, Eskelinen EL, Fujita H, Saftig P, Himeno M, Tanaka Y. 2002. A role for the lysosomal membrane protein LGP85 in the biogenesis and maintenance of endosomal and lysosomal morphology. *J Cell Sci* 115:4117–4131. <https://doi.org/10.1242/jcs.00075>.
- Reczek D, Schwake M, Schroder J, Hughes H, Blanz J, Jin X, Brondyk W, Van Patten S, Edmunds T, Saftig P. 2007. LIMP-2 is a receptor for lysosomal mannose-6-phosphate-independent targeting of beta-glucocerebrosidase. *Cell* 131:770–783. <https://doi.org/10.1016/j.cell.2007.10.018>.
- Yamayoshi S, Iizuka S, Yamashita T, Minagawa H, Mizuta K, Okamoto M, Nishimura H, Sanjoh K, Katsushima N, Itagaki T, Nagai Y, Fujii K, Koike S. 2012. Human SCARB2-dependent infection by coxsackievirus A7, A14, and A16 and enterovirus 71. *J Virol* 86:5686–5696. <https://doi.org/10.1128/JVI.00020-12>.
- Yamayoshi S, Koike S. 2011. Identification of a human SCARB2 region that is important for enterovirus 71 binding and infection. *J Virol* 85:4937–4946. <https://doi.org/10.1128/JVI.02358-10>.
- Yamayoshi S, Ohka S, Fujii K, Koike S. 2013. Functional comparison of SCARB2 and PSGL1 as receptors for enterovirus 71. *J Virol* 87:3335–3347. <https://doi.org/10.1128/JVI.02070-12>.
- Jiao XY, Guo L, Huang DY, Chang XL, Qiu QC. 2014. Distribution of EV71 receptors SCARB2 and PSGL-1 in human tissues. *Virus Res* 190:40–52. <https://doi.org/10.1016/j.virusres.2014.05.007>.
- Wang SM, Ho TS, Lin HC, Lei HY, Wang JR, Liu CC. 2012. Reemerging of enterovirus 71 in Taiwan: the age impact on disease severity. *Eur J Clin Microbiol Infect Dis* 31:1219–1224. <https://doi.org/10.1007/s10096-011-1432-6>.
- Fujii K, Nagata N, Sato Y, Ong KC, Wong KT, Yamayoshi S, Shimanuki M, Shitara H, Taya C, Koike S. 2013. Transgenic mouse model for the study of enterovirus 71 neuropathogenesis. *Proc Natl Acad Sci U S A* 110:14753–14758. <https://doi.org/10.1073/pnas.1217563110>.
- Yang CH, Liang CT, Jiang ST, Chen KH, Yang CC, Cheng ML, Ho HY. 2019. A novel murine model expressing a chimeric mSCARB2/hSCARB2 receptor is highly susceptible to oral infection with clinical isolates of enterovirus 71. *J Virol* 93:e00183-19. <https://doi.org/10.1128/JVI.00183-19>.
- Huang R, Guo G, Lu L, Fu R, Luo J, Liu Z, Gu Y, Yang W, Zheng Q, Chao T, He L, Wang Y, Niu Z, Wang H, Lawrence T, Malissen M, Malissen B, Liang Y, Zhang L. 2019. The three members of the Vav family proteins form complexes that concur to foam cell formation and atherosclerosis. *J Lipid Res* 60:2006–2019. <https://doi.org/10.1194/jlr.M094771>.
- Wang X, Huang R, Zhang L, Li S, Luo J, Gu Y, Chen Z, Zheng Q, Chao T, Zheng W, Qi X, Wang L, Wen Y, Liang Y, Lu L. 2018. A severe atherosclerosis mouse model on the resistant NOD background. *Dis Model Mech* 11:dmm033852. <https://doi.org/10.1242/dmm.033852>.
- Chao T, Liu Z, Zhang Y, Zhang L, Huang R, He L, Gu Y, Chen Z, Zheng Q, Shi L, Zheng W, Qi X, Kong E, Zhang Z, Lawrence T, Liang Y, Lu L. 2019. Precise and rapid validation of candidate gene by allele specific knockout with CRISPR/Cas9 in wild mice. *Front Genet* 10:124. <https://doi.org/10.3389/fgene.2019.00124>.
- Nishimura Y, Shimojima M, Tano Y, Miyamura T, Wakita T, Shimizu H. 2009. Human P-selectin glycoprotein ligand-1 is a functional receptor for enterovirus 71. *Nat Med* 15:794–797. <https://doi.org/10.1038/nm.1961>.
- Huang H, Shih SR. 2015. Neurotropic enterovirus infections in the central nervous system. *Viruses* 7:6051–6066. <https://doi.org/10.3390/v7112920>.

28. Wong KT, Munisamy B, Ong KC, Kojima H, Noriyo N, Chua KB, Ong BB, Nagashima K. 2008. The distribution of inflammation and virus in human enterovirus 71 encephalomyelitis suggests possible viral spread by neural pathways. *J Neuropathol Exp Neurol* 67:162–169. <https://doi.org/10.1097/nen.0b013e318163a990>.
29. Huang CC, Liu CC, Chang YC, Chen CY, Wang ST, Yeh TF. 1999. Neurologic complications in children with enterovirus 71 infection. *N Engl J Med* 341:936–942. <https://doi.org/10.1056/NEJM199909233411302>.
30. Nagata N, Shimizu H, Ami Y, Tano Y, Harashima A, Suzaki Y, Sato Y, Miyamura T, Sata T, Iwasaki T. 2002. Pyramidal and extrapyramidal involvement in experimental infection of cynomolgus monkeys with enterovirus 71. *J Med Virol* 67:207–216. <https://doi.org/10.1002/jmv.2209>.
31. Chang LY, Huang LM, Gau SS, Wu YY, Hsia SH, Fan TY, Lin KL, Huang YC, Lu CY, Lin TY. 2007. Neurodevelopment and cognition in children after enterovirus 71 infection. *N Engl J Med* 356:1226–1234. <https://doi.org/10.1056/NEJMoa065954>.
32. Lin YW, Yu SL, Shao HY, Lin HY, Liu CC, Hsiao KN, Chitra E, Tsou YL, Chang HW, Sia C, Chong P, Chow YH. 2013. Human SCARB2 transgenic mice as an infectious animal model for enterovirus 71. *PLoS One* 8:e57591. <https://doi.org/10.1371/journal.pone.0057591>.
33. Liao CC, Liou AT, Chang YS, Wu SY, Chang CS, Lee CK, Kung JT, Tu PH, Yu YY, Lin CY, Lin JS, Shih C. 2014. Immunodeficient mouse models with different disease profiles by in vivo infection with the same clinical isolate of enterovirus 71. *J Virol* 88:12485–12499. <https://doi.org/10.1128/JVI.00692-14>.
34. Jin Y, Zhang C, Wang H, Zhou G, Wang X, Zhang R, Chen S, Ren J, Chen L, Dang D, Zhang P, Xi Y, Wu W, Zhang W, Duan G. 2018. Mast cells contribute to enterovirus 71 infection-induced pulmonary edema in neonatal mice. *Lab Invest* 98:1039–1051. <https://doi.org/10.1038/s41374-018-0075-y>.
35. Xiu JH, Zhu H, Xu YF, Liu JN, Xia XZ, Zhang LF. 2013. Necrotizing myositis causes restrictive hypoventilation in a mouse model for human enterovirus 71 infection. *Virology* 452:215. <https://doi.org/10.1016/j.virol.2013.10.015>.
36. Lin W, Su Y, Jiang M, Liu J, Zhang YY, Nong GM. 2017. Clinical features for 89 deaths of hand, foot and mouth disease in Guangxi, China, 2014. *Int J Infect Dis* 64:15–19. <https://doi.org/10.1016/j.ijid.2017.08.016>.
37. Rahimi R, Omar E, Tuan Soh TS, Mohd Nawi SFA, Md Noor S. 2017. A sudden paediatric death due to hand, foot and mouth disease: the importance of vigilance. *Malays J Pathol* 39:167–170.
38. Chang LY, Huang YC, Lin TY. 1998. Fulminant neurogenic pulmonary oedema with hand, foot, and mouth disease. *Lancet* 352:367–368. [https://doi.org/10.1016/S0140-6736\(98\)24031-1](https://doi.org/10.1016/S0140-6736(98)24031-1).
39. Forrester JV, McMenamin PG, Dando SJ. 2018. CNS infection and immune privilege. *Nat Rev Neurosci* 19:655–671. <https://doi.org/10.1038/s41583-018-0070-8>.
40. Feng M, Guo S, Fan S, Zeng X, Zhang Y, Liao Y, Wang J, Zhao T, Wang L, Che Y, Wang J, Ma N, Liu L, Yue L, Li Q. 2016. The preferential infection of astrocytes by enterovirus 71 plays a key role in the viral neurogenic pathogenesis. *Front Cell Infect Microbiol* 6:192. <https://doi.org/10.3389/fcimb.2016.00192>.
41. Yu L, He J, Wang L, Yi H. 2019. Inflammatory profiles revealed the dysregulation of cytokines in adult patients of HFMD. *Int J Infect Dis* 79:12–20. <https://doi.org/10.1016/j.ijid.2018.11.001>.
42. Zhang W, Huang Z, Huang M, Zeng J. 2020. Predicting severe enterovirus 71-infected hand, foot, and mouth disease: cytokines and chemokines. *Mediators Inflamm* 2020:9273241. <https://doi.org/10.1155/2020/9273241>.
43. Merle NS, Church SE, Fremeaux-Bacchi V, Roumenina LT. 2015. Complement system, part I—molecular mechanisms of activation and regulation. *Front Immunol* 6:262. <https://doi.org/10.3389/fimmu.2015.00262>.
44. Qiu S, Liu N, Jia L, Yang G, Su W, Li J, Song L, Yang C, Wang J, Zhang C, Wang Z, Qiao F, Tomlinson S, Atkinson C, Sun Y, Huang L, Song H, Wang Y, Li Z. 2012. A new treatment for neurogenic inflammation caused by EV71 with CR2-targeted complement inhibitor. *Virology* 439:285. <https://doi.org/10.1016/j.virol.2012.09.025>.
45. Farber JM. 1997. Mig and IP-10: CXC chemokines that target lymphocytes. *J Leukoc Biol* 61:246–257. <https://doi.org/10.1002/jlb.61.3.246>.
46. Suzuki K, Nakaji S, Yamada M, Totsuka M, Sato K, Sugawara K. 2002. Systemic inflammatory response to exhaustive exercise. Cytokine kinetics. *Exerc Immunol Rev* 8:6–48.
47. Bui TM, Wiesolek HL, Sumagin R. 2020. ICAM-1: a master regulator of cellular responses in inflammation, injury resolution, and tumorigenesis. *J Leukoc Biol* 108:787–799. <https://doi.org/10.1002/JLB.2MR0220-549R>.
48. Dang D, Zhang C, Zhang R, Wu W, Chen S, Ren J, Zhang P, Zhou G, Feng D, Sun T, Li Y, Liu Q, Li M, Xi Y, Jin Y, Duan G. 2017. Involvement of inducible nitric oxide synthase and mitochondrial dysfunction in the pathogenesis of enterovirus 71 infection. *Oncotarget* 8:81014–81026. <https://doi.org/10.18632/oncotarget.21250>.